2014

Adaptive Mechanical Properties of Topologically Interlocking Material Systems

S Khandelwal

Thomas Siegmund
Purdue University, siegmund@purdue.edu

R J. Cipra

J S. Bolton

Adaptive Mechanical Properties of Topologically Interlocking Material Systems

S. Khandelwal [†], T. Siegmund [†] *, R. J. Cipra [†], J. S. Bolton [‡],

School of Mechanical Engineering

[†] 585 Purdue Mall, Purdue University, West Lafayette, IN-47907, USA

[‡] Ray W. Herrick Laboratories, 140 S. Martin Jischke Drive, Purdue University, West Lafayette, IN-47907, USA

*Corresponding author, email: siegmund@purdue.edu, phone (765) 494 9766

ABSTRACT:

Topologically interlocked material systems are two-dimensional granular crystals created as ordered and adhesion-less assemblies of unit elements of the shape of platonic solids. The assembly resists transverse forces due to the interlocking geometric arrangement of the unit elements. Topologically interlocked material systems yet require an external constraint to provide resistance under the action of external load. Past work considered fixed and passive constraints only. The objective of the present study is to consider active and adaptive external constraints with the goal to achieve variable stiffness and energy absorption characteristics of the topologically interlocked material system through an active control of the in-plane constraint conditions. Experiments and corresponding model analysis are used to demonstrate control of system stiffness over a wide range, including negative stiffness, and energy absorption characteristics. The adaptive characteristics of the topologically interlocked material system are shown to solve conflicting requirements of simultaneously providing energy absorption while keeping loads controlled. Potential applications can be envisioned in smart structure enhanced response characteristics as desired in shock absorption, protective packaging and catching mechanisms.

Keywords: Topologically Interlocked Material Systems, Granular Crystals, Adaptive Energy Absorption, Adaptive Stiffness, Smart Material Systems.

Adaptive Mechanical Properties of Topologically Interlocking Material Systems

1. INTRODUCTION

Hybrid material systems combine the attributes of the three main pillars of materials engineering - chemistry to create new compounds, microstructure design, and microarchitecture ([1]-[5]) – with the goal to achieve new performance profiles. Active material concepts further expand the space of accessible response characteristics ([6]-[10]). Active material concepts also enable the response to external stimuli and a given material system thus can occupy separate locations in the material property space at different times. The selection of the specific strategy for designing materials is primarily determined by the required functional performance ([11], [12]). Here, the focus is on a novel material system concept with adaptive control of stiffness and energy absorption.

The ability of to prevent damage to life and property is an important performance consideration in designing protective structures. Two potentially conflicting characteristics have thereby to be fulfilled, i.e. that of large energy absorption and low stress levels. Consequently, a protective structure ideally allows a large amount of deformations under a limited level of stress. Typically, such characteristics have been achieved utilizing structural plastic collapse mechanisms of thin walled metallic structures and structural crushing of composite structures, as well as microstructure level plastic collapse or crushing in honeycombs and foams ([13]-[20]). However, these systems are passive. Therefore, the systems are used either in a non-optimal context, or to optimally response to given target stress and energy absorption levels have to be created individually for each loading condition. In order to alleviate such restrictions, adaptive energy absorbers have been considered.

Relevant concepts of adaptive energy absorbers have been based on hydraulic damper elements controlling the different segments of an energy absorbing structure ([21], [22]), the use of shape memory alloy (SMA) elements ([23], [24]) and the use of magneto-rheological (MR) fluids ([25], [26]). Holnicki-Szulc et al. [24] conceptually modeled and analyzed an adaptive energy absorption system with variable yield strength using sequentially collapsing micro-trusses connected with SMA based micro-fuses. Deshmukh and McKinley [27] created and analyzed adaptive energy absorbing cellular solids whose mechanical properties were modulated by impregnating them with MR fluids that change their stiffness by shear thickening upon application of the magnetic field. The energy absorption capacity for the proposed material was seen to vary 50 fold by changing the magnetic field. A scaling model was also proposed to model the fluid-solid composite behavior. The model was then used to optimize the material system properties based on application requirements such as headrest with no whiplash. In [28] a theoretical analysis of MR based energy absorbers was conducted with the objective to obtain the optimal system parameters for achieving a soft landing i.e. where the payload comes to rest at the end of the stroke with no large crushing forces as obtained for foams. The optimal Bingham number minimizing

drop-induced shock loads utilizing large damper strokes was obtained for the MR fluid based smart material system.

In this study an alternative strategy for creating material systems with adaptive response characteristics is pursued. The concept of Topologically Interlocking Material (TIM) systems is followed. TIM systems are 2D granular crystals created as assemblies of unit elements of the shape of platonic solids. The assembly resists transverse forces due to the interlocking geometric arrangement of the unit elements. As adhesionless granular system, TIMs require an external constraint to provide resistance under the action of external load. TIM systems have already been shown to possess attractive mechanical properties including: (i) high damage tolerance ([29]-[31]), (ii) negative stiffness characteristics under certain loading conditions ([32], [33]), (iii) a quasi-ductile mechanical response response even if constituent materials are brittle ([29], [34]-[36]), (iv) remanufacturability [37], and (v) advantageous dependence of stiffness, strength and toughness with variation in relative density if cellular unit elements are considered [38]. Past work has demonstrated the effect of change of the initial constraint conditions on the TIM system stiffness and load carrying capacity. Schaare et al. [33] – employing finite element (FE) simulations -- showed that the mechanical resistance of a simulated TIM system was proportional to the constraint conditions. TIM assemblies can be seen as a special class of granular materials. These material systems are well known to possess pressure dependent characteristics [39]. This insight has been used to create adaptive response characteristics for robotic grippers [40] or malleable and shape-changing devices [41]. Load transfer in granular media can be analyzed via force chains ([42], [43]). Extending concept of the force chain analysis, in [38] and [44] the mechanical properties of TIM assemblies were analyzed.

The present study is concerned with the adaptive response of TIM assemblies under quasi-static loading. The active control of the resistance to out-of- loading is demonstrated, and adaptive changes to the energy absorption capacity are demonstrated. Experiments were performed to simultaneously measure the transverse force in response to an applied displacement, and in-plane confinement force while maintaining a predetermined stiffness over large deformations. Positive, zero and negative stiffness responses are demonstrated. An analytical model capturing the deformation characteristics of TIM assemblies based on earlier work ([38], [44]) was established to incorporate active control. The computational code for this model was used to calculate the TIM system response, and model results are compared with experiments.

2. MATERIAL and METHODS

Topologically interlocked material assemblies were created from regular tetrahedral unit elements. The edge length of the tetrahedral elements was $a_0 = 25.00$ mm . Unit elements, as well as the abutments used for confining the assembly, were manufactured in a 3D printer, Dimension SST 1200 (Stratasys Inc.), by fused deposition processing of a polymer (ABS P400) with a print layer thickness of 0.25 mm. The room temperature elastic modulus of the printed polymer is $E_S = 1827.0$ MPa. All experiments were conducted at room temperature, significantly below the glass transition temperature of the polymer, and time dependent deformation processes were negligible.

Monolayers of the topologically interlocked material assembly consisted of 49 identical tetrahedra in a dense 2D packing in the shape of a square lattice pattern [45]. Each tetrahedron was supported by four surrounding tetrahedra, two in each lateral direction preventing motion in either transverse direction, Figure 1(a). The assembled monolayer specimens possessed an edge length at the top and bottom surfaces of $L_{\mathrm{U}} = (N+1)a_0/2 = 100.00$ mm. The mid-plane section was a square of edge-length $L_0 = Na_0/2 =$ 87.50 mm. The effective thickness of the monolayer was $h = a_0/\sqrt{2} = 17.68$ mm equal to the edge-to-edge distance in the unit tetrahedron. The assembly process was facilitated by the use of a template consisting of 8×8 square pyramids arranged on a square grid. Subsequently, the assembled monolayer was confined by the use of abutments placed along its edges, Figure 1(b). The abutments were of prismatic shape and possessed a wedge shape cross-section enabling the engagement of the abutment with the monolayer, Figure 1(c).

TIM assemblies were placed into a rigid test frame, Figure 1(b). Two adjacent abutments were fixed in space while the two opposing abutments possess a degree of freedom in the assembly plane in the direction orthogonal to the axis of the respective abutments. The in-plane actuation enables the control of the confinement of the TIM assemblies. Actuation was achieved by the use of a pair of screws (Zinc-Plated alloy steel socket head cap screw 3/8"-16 thread, 2" length) per movable abutment. These screws acted onto steel shims inserted between the movable abutments and the rigid test frame. The in-plane confinement forces were measured by using thin film force sensors (FlexiForce Model A201) placed between the fixed abutments and the test frame. These abutments possessed two cylindrical extrusions on the back face, each of diameter equal to that of the force sensor. Each sensor possessed a maximum load rating of 50.00 N such that a maximum in-plane confinement force of 100.00 N was possible. The in-plane force F_{H} was reported as the average of the force readings measured in the two in-plane directions.

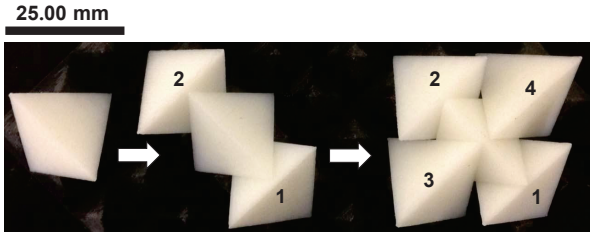

(a)

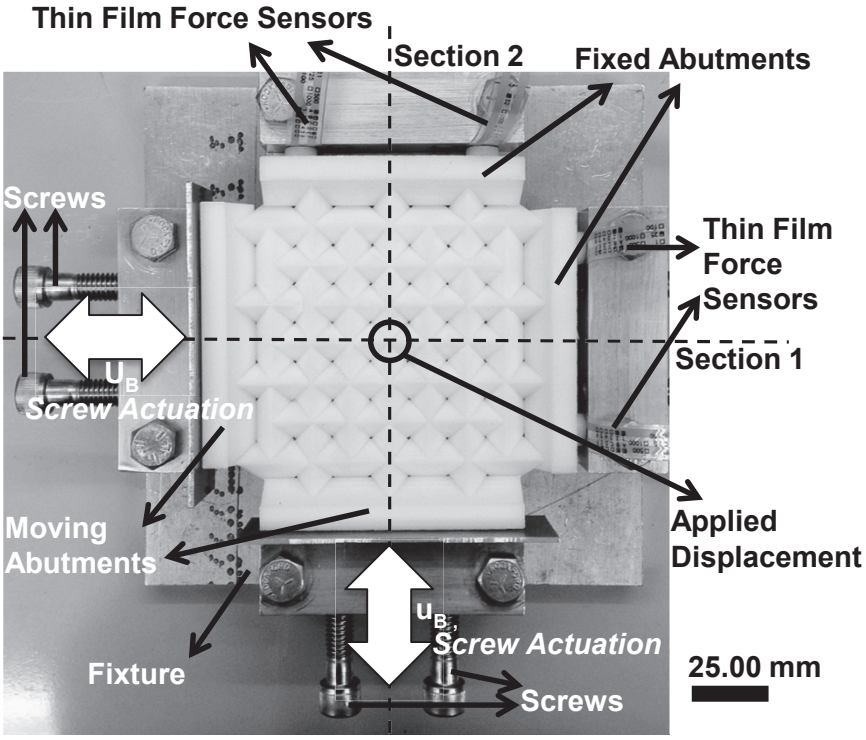

(b)

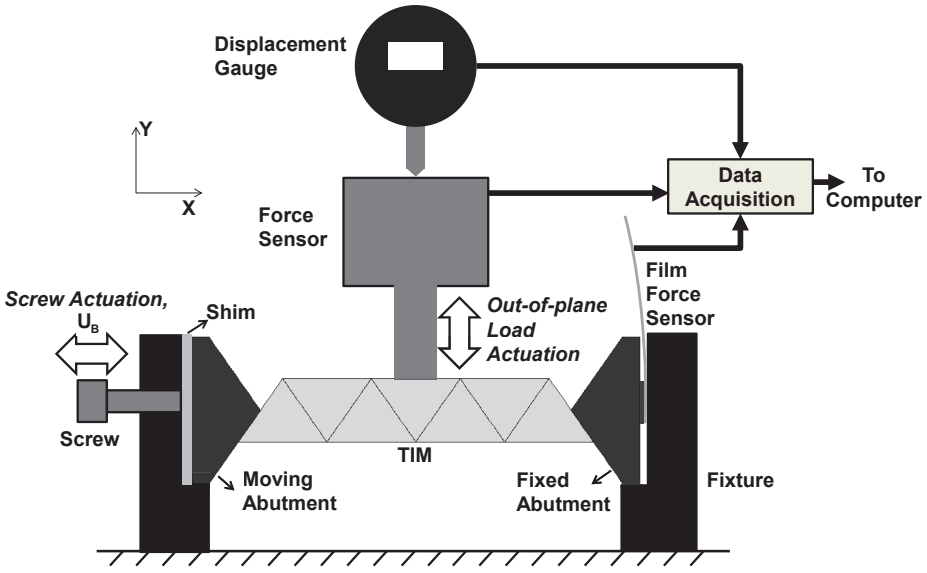

(c)

Figure 1: (a) Interlocking arrangement of individual elements, (b) Top view of topologically interlocked material assembly in test frame, and (c) Schematic of the test set-up. Double-headed arrows show the direction of motion of actuation.

All experiments consider an initial condition with a small in-plane preload, $F_{H0} = 8.00$ N. Once the constraint was set, specimens were placed in the test system, Figure 1(c), such that a transverse displacement was applied to the three centrally located tetrahedra, Figure 1(b). The mechanical test system was assembled using a manually actuated translation stage, a load cell (range: 50.00 N, sensitivity: 0.002 N, PASCO scientific) and a displacement gauge (range: 0.00 mm – 50.00 mm, sensitivity: 0.001 mm, PASCO scientific). Transverse force, applied displacement, and in-plane forces were recorded concurrently at a frequency of 5.00 Hz.

The transverse load is applied in displacement control via an indenter type load applied to the center of the assembly. Under initially fixed in-plane constraint the TIM assemblies were loaded until the corresponding out-of-plane force reached a specified value F_c at displacement $\delta^{\perp}$. Upon loading beyond F_c, the in-plane constraint was reduced such that the desired transverse stiffness response K_T was obtained. For a desired stiffness response K_T, one obtains a target force response F_T at a given applied displacement δ as $F_T = F_c + K_T(\delta - \delta^{\perp})$. If the actual out-of-plane force F differed from the desired target response F_T by more than the defined tolerance $\Delta F = \pm 5.00$ N, the in-plane load constraint was altered by further displacement of the abutments so as to obtain the required force response.

Experiments considered positive stiffness ($K_T = K_T^+ = +1.50$ N/mm, zero stiffness ($K_T = K_T^0 = 0.0$ N/mm), and negative stiffness ($K_T = K_T^-$ = -2.5 N/mm). Data primarily considered $F_c = 30.00$ N. Results for K_T^0 are also shown for $F_c = 20.00$ N. For each load cases considered, four repeat experiments were performed.

3. MODEL

In an ordered granular system, such as in a TIM assembly, the geometry of the force chains (or thrust lines) can be established deterministically. Recognizing the static indeterminacy of the problem at hand, a framework for the predictions of the mechanical properties of TIM assemblies was developed in [38]. Here this concept is expanded to TIM assemblies with active control.

Figure 2(a) shows the TIM in isometric view. Figure 2(b) shows the section views for the planes of type 1 and 2 marked in Figure 2(a). A transverse displacement δ is applied centrally to the TIM in the –Y

direction. For section of type P_1, tetrahedra adjacent to the abutments are constraint against rotation by the constraint imposed by the abutments. Thus, elements located in a section P_1 can transfer compressive forces to the abutments. As tetrahedra interact with each other and with the abutments by contact only, the location of the force chain can be established. Force chains are established between the central tetrahedron (the point of load application) and the point of contact between abutment and adjacent tetrahedra. Force chains are orthogonal to the tetrahedra-to-tetrahedra contact. For section of type P_2, the abutments do not restrict the rotation of tetrahedra adjacent to the abutments and no loads are transferred for loading in the -Y direction. The situation between P_1 and P_2 is reversed for loads applied in the +Y direction. P_1 and P_2 are called thrust planes.

This model is captured in Figure 3, which shows the conditions for a thrust plane of the type section 1 for external loads in -Y. It is assumed that thrust lines can be modeled as trusses connected by hinges. The final model consists of three trusses. The first truss extents from the contact point between abutment and tetrahedron (X_1) to the center tetrahedron (X_2), a second truss represents the center tetrahedron (X_2 to X_3), and a third truss is located between the center tetrahedron and the abutment (X_3 to X_4). Since there are several planes of type P_1, each such thrust plane contributes additively to the overall force as reaction to the applied displacement. Further details of the model are documented in [38].

In the experiment the applied in-plane displacement U_B, is non-symmetric with regards to the TIM assembly center. In the model, in order to solve the model efficiently and since U_B is much smaller than L_0, a symmetric configuration is considered, Figure 3. Then, the in-plane displacement to change the constraint is applied as $u_B = U_B / 2$ at location X_1, and simultaneously as $-u_B$ at location X_4.

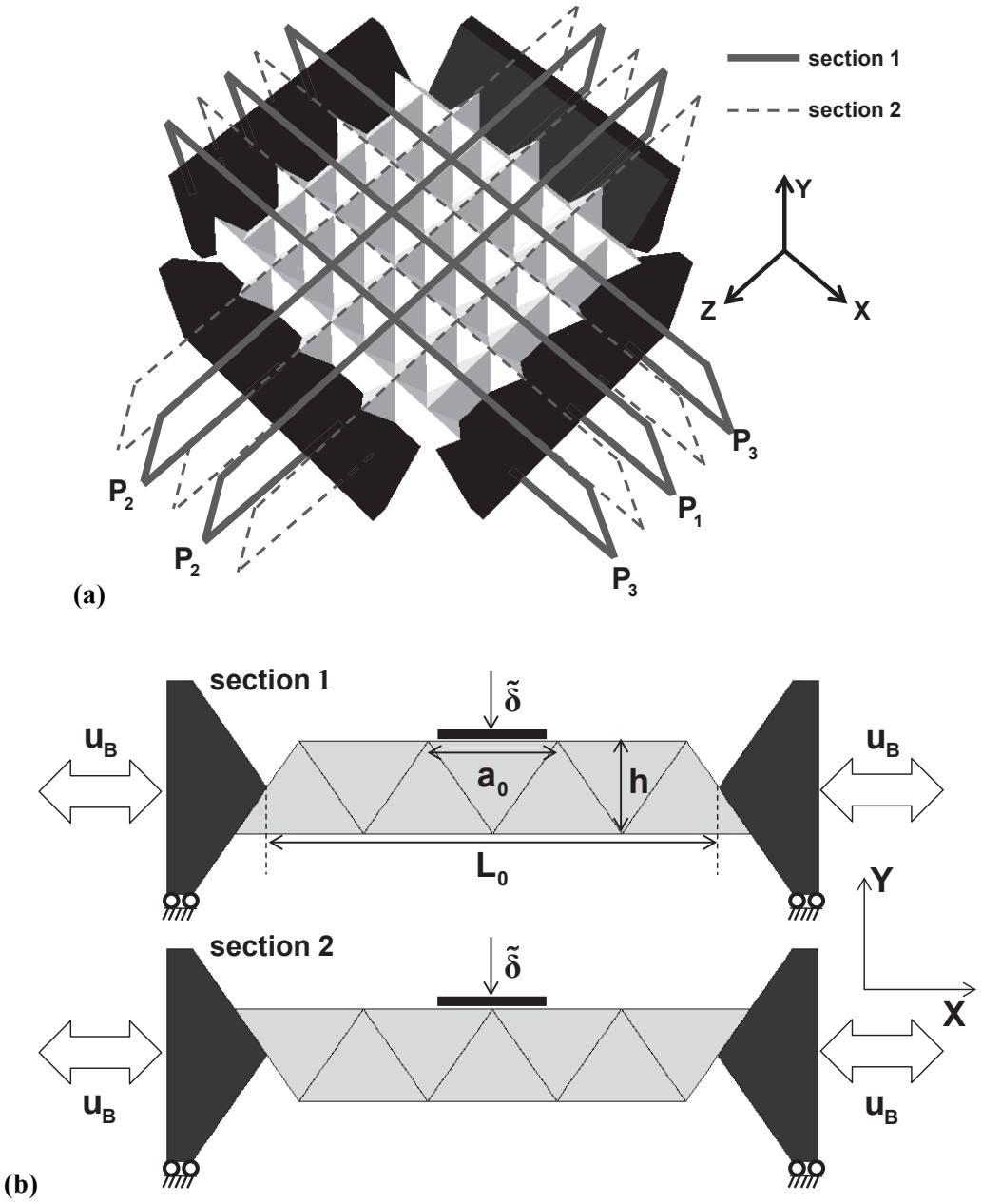

Figure 2: (a) A representative TIM with the two alternating cross-section planes marked. (b) The two characteristic and alternating cross-sections present in the TIM assembly.

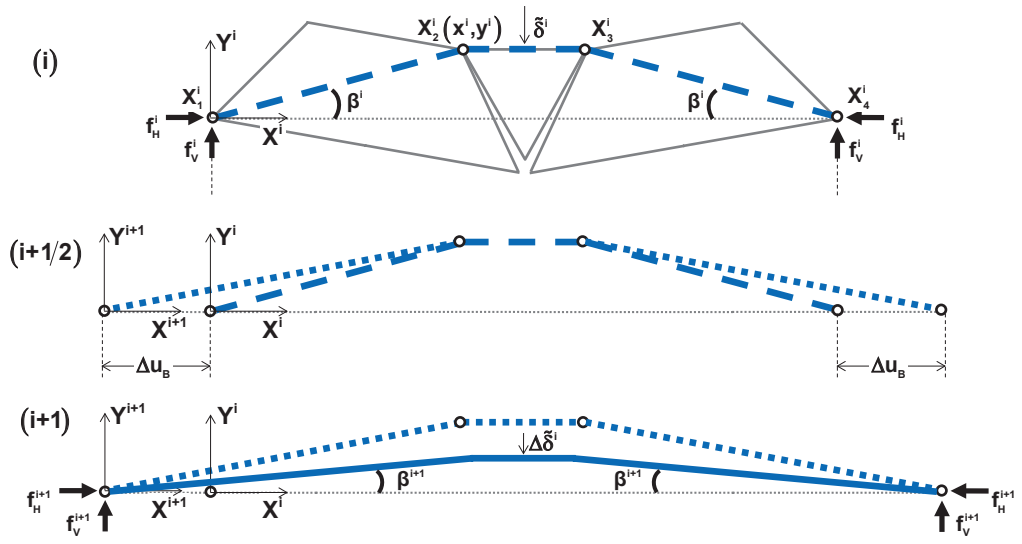

Figure 3: Thrust lines for TIM assemblies and change in in-plane constraint and increase in applied displacement: From configuration (i) at high constraint and before increase in applied displacement to configuration (i+1/2) with a reduced constraint and (i+1) with new displacement increment applied to the new constraint situation.

Consider a thrust plane of type P_1 where an increment of displacement $\Delta\tilde{\delta}^i$ is prescribed at the center in increment (i), Figure 3. The force response is obtained as:

$$\frac{\Delta f_H^i}{EA} = \left[\frac{x_0^i}{\sqrt{\left(x_0^i\right)^2+\left(y_0^i\right)^2}}\right]\left[\frac{\sqrt{\left(x_0^i\right)^2+\left(y_0^i\right)^2}}{\sqrt{\left(x_0^i\right)^2+\left(y_0^i-\Delta\tilde{\delta}^i\right)^2}}-1\right] \quad , \quad f_H^i = \sum_0^i \Delta f_H \tag{1a}$$

$$\frac{\Delta f_V^i}{EA} = \frac{\Delta f_H^i}{EA}\tan\beta^i = \left[\frac{x_0^i}{\sqrt{\left(x_0^i\right)^2+\left(y_0^i\right)^2}}\right]\left[\frac{\sqrt{\left(x_0^i\right)^2+\left(y_0^i\right)^2}}{\sqrt{\left(x_0^i\right)^2+\left(y_0^i-\Delta\tilde{\delta}^i\right)^2}}-1\right]\left(\frac{y_0^i-\Delta\tilde{\delta}^i}{x_0^i}\right) \quad , \quad f_V^i = \sum_0^i \Delta f_V \tag{1b}$$

where f_H^i and f_V^i are the in-plane and out-of-plane forces, respectively, generated in the thrust plane, and β^i is the inclination of truss X_1X_2 (and similarly, X_3X_4) with regard to the assembly plane. Furthermore, (x_0^i, y_0^i) are the co-ordinates of X_2, A is an equivalent cross-section area of the truss representing the thrust line and E is the Young's modulus of the material of which the unit elements in the assembly are made. At increment (i) the out-of-plane force for the overall assembly F^i is obtained as

$$\frac{F^i}{EA} = 2\frac{f_V^i\left(P_1\right)}{EA} + 4\sum_{i=2}^{(N-1)/2}\frac{f_V^i\left(P_m\right)}{EA} \tag{2}$$

where $f_{\mathrm{V}}^{\mathrm{i}}(P_{\mathrm{m}})$ and $f_{\mathrm{H}}^{\mathrm{i}}(P_{\mathrm{m}})$ denote respectively the out-of-plane and in-plane force generated in the m^{th} thrust plane P_{m}. In a TIM assembly made of $N \times N$ unit elements one defines $m = 1,2,\ldots,(N-1)/2$ with $m = 1$ being the central plane and $m = (N-1)/2$ being the outermost plane. The displacement $\tilde{\delta}(P_{\mathrm{m}})$ of the central tetrahedron in each plane P_{m} relates to the applied displacement δ as:

$$\tilde{\delta}(P_{\mathrm{m}}) = \left[\frac{\frac{(N+1)}{2} - (m-1)}{\frac{(N+1)}{2}} \right] \delta \,. \tag{3}$$

At any given increment (i) the transverse stiffness $K = dF / d\delta$ of the TIM assembly is obtained by backward numerical differentiation:

$$K^{\mathrm{i}} = \frac{F^{\mathrm{i}} - F^{\mathrm{i-1}}}{\delta^{\mathrm{i}} - \delta^{\mathrm{i-1}}} \,. \tag{4}$$

Considering active control of a target force F_{T}, the in-plane displacement $u_{\mathrm{B}}^{\mathrm{i+1}}$ at increment (i+1) is updated using the following rule:

$$u_{\mathrm{B}}^{\mathrm{i+1}}\left(\tilde{\delta} + \Delta\tilde{\delta}\right) = \begin{cases} u_{\mathrm{B}}^{\mathrm{i}}\left(\tilde{\delta}\right) - \Delta u_{\mathrm{B}} & \text{if} \quad \dfrac{F^{\mathrm{i}}}{F_{\mathrm{T}}} > \in_{\mathrm{K}} \\ u_{\mathrm{B}}^{\mathrm{i}}\left(\tilde{\delta}\right) & \text{if} \quad \dfrac{F^{\mathrm{i}}}{F_{\mathrm{T}}} < \in_{\mathrm{K}} \end{cases} \tag{5}$$

where $\in_{\mathrm{K}} > 1.00$ is a tolerance on the target force F_{T}. If the force F^{i} is greater than the target force, F_{T}, by a tolerance of $\in_{\mathrm{K}}$, then the constraint is relaxed and abutments are displaced by Δu_{B}. Here, cases with increasing system stiffness were not considered.

The model was solved explicitly with the in-plane constraint updated before the forces at increment (i+1) were obtained. This can be thought of as being a computation is two half-steps, Figure 3, such that at (i+1/2) the truss end points were displaced by Δu_{B} and subsequently kept fixed at (i+1). At increment (i+1) one thus obtains

$$\left[x_0^{\mathrm{i+1}}\left(\mathrm{X}_{\mathrm{i+1}}, \mathrm{Y}_{\mathrm{i+1}}\right), y_0^{\mathrm{i+1}}\left(\mathrm{X}_{\mathrm{i+1}}, \mathrm{Y}_{\mathrm{i+1}}\right) \right] = \left[x^{\mathrm{i}}\left(\mathrm{X}_{\mathrm{i}}, \mathrm{Y}_{\mathrm{i}}\right) + \Delta u_{\mathrm{B}}, y^{\mathrm{i}}\left(\mathrm{X}_{\mathrm{i+1}}, \mathrm{Y}_{\mathrm{i+1}}\right) \right]. \tag{6}$$

The updated (x_0^{i+1}, y_0^{i+1}) were then incorporated in Eqs. (1a,b) and the total out-of-plane force response was subsequently obtained using Eq. (2). This process was repeated until the final collapse of the assembly ($F = 0$ at a displacement $\delta = \delta_f$). The in-plane constraint force F_H was not restricted to reach zero at this instance. The model provides normalized force response, F_V / EA and F_H / EA as output and was calibrated with a physical experiment with EA=1.52 N. This calibration is based on data documented in [38] where all experiments considered a fixed constraint with zero in-plane preload. Computations were conducted with numerical parameters $\in_K = 1.05$ and $\Delta u_B = 0.02$ mm . The system was controlled within a tolerance of ± 5.00 N from the desired force level.

4. RESULTS

A representative $F - \delta$ response curves are depicted in Figure 4. The response of a TIM under fixed constraint conditions, data from [38], demonstrates a characteristic parabolic response with the TIM exhibiting a gradual decay in load carrying capacity until final collapse.

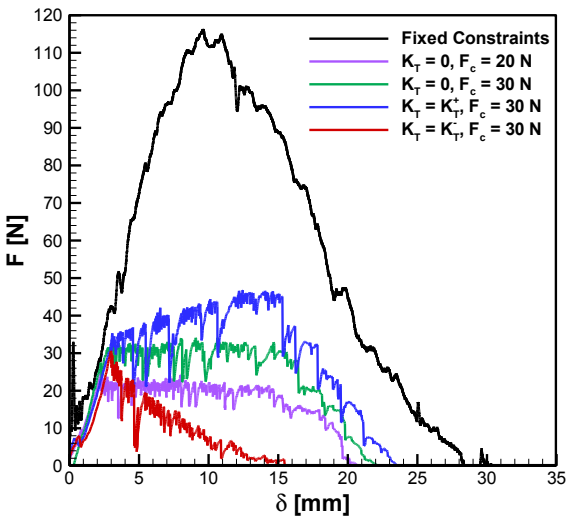

Figure 4: Measured $F - \delta$ response for the physical experiments with controlled constraints. Response obtained from material with fixed constraints [38] gives the envelope of available $F - \delta$ space.

For each of adaptively controlled load cases considered in the present study on representative result is shown in Figure 5. These data demonstrate that the proposed adaptive control of the TIM response can indeed be realized experimentally. For the adaptively controlled samples, the adjustment of the in-plane constraint was initiated once F_c was reached. The subsequent $F - \delta$ response exhibits two characteristic

points. It was found that past a critical deflection δ_c (its value dependent on F_c and K_T) the load carrying capacity of the TIMs could not be maintained at the desired value, and that all load carrying capacity vanishes at δ_f. For TIMs with variable constraints the values of deflection δ_f were found to be less than that observed for the experiment with fixed constraints. The lower the average constraint the larger is that deviation, therefore this observation is contributed to slip between unit elements which is enabled more significantly under low confinement. Four repeats of each experimental condition (K_T^+, K_T^0 and K_T^-) were conducted. Figure 5 shows both out-of-plane and corresponding in-plane forces in dependence of the applied displacement. Figure 5(a) also indicates the two characteristic deflection values δ_c and δ_f in a general sense. For experiments with K_T^0, the in-plane constraint forces required to maintain a constant transverse load initially rise only marginally, but towards higher applied displacement an increase in constraint is required to maintain the desired response. Maintaining K_T^+ requires a continuous increase in the in-plane constraint, yet the rate of increase in constraint clearly is lower than during the stage where the abutments are fixed in the initial position. The most readily controllable case is the one of K_T^- for which in-plane confinement forces actually decline with increase in applied displacement.

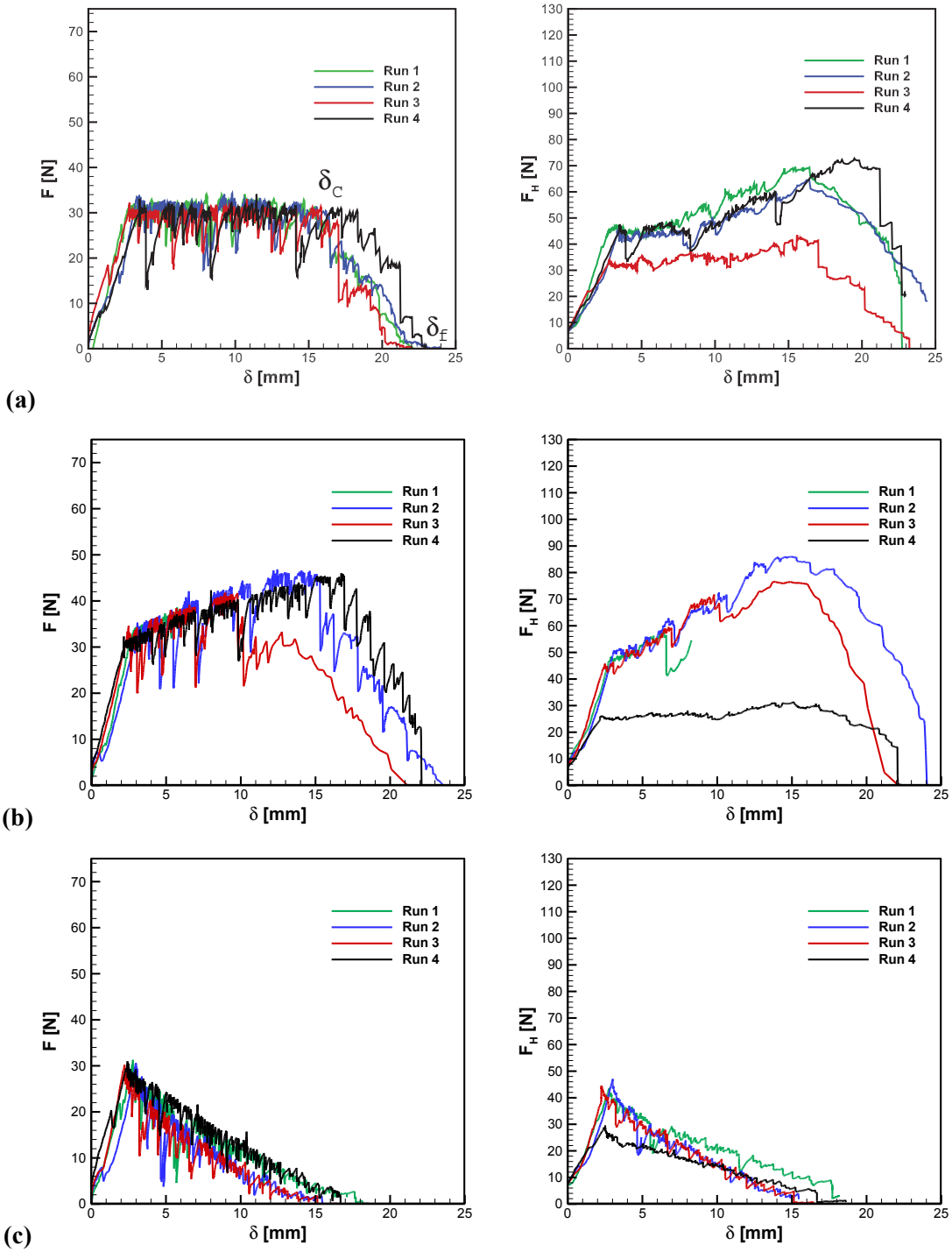

Figure 5: Repeatability of experiments for the three load cases discussed in the study, (a) $K = 0.00$ N/mm, (b) $K_T = K_T^+$, (c) $K_T = K_T^-$. In (a) to (c) each pair of graphs depicts out-of-plane force F and corresponding in-plane force F_H, respectively. In-plane force sensors failed during Run 4 for $K_T = K_T^+$.

Figure 6 compares experimental data and model predictions for K_T^0 and $F_c = 20.00$ N and 30.00 N with (a) – (b) depicting corresponding out-of-plane force data and (c) – (d) depicting respective in-plane force data. Overall, experiment and model are in good agreement, especially up to deflection δ_c. This is however not the case for the late stages of the load history. In the experiment, final failure is at δ_f ~22.0 mm. The model, however, predicts δ_f =35.0 mm corresponding to $\delta_f = 2h$ [38]. Conversely, the predicted in-plane force response continues to increase to larger values than measured and the final break down is shifted to larger applied displacements. Again, the difference is contributed to slip between tetrahedra which is not accounted in the model. Yet, qualitative predictions are in excellent agreement.

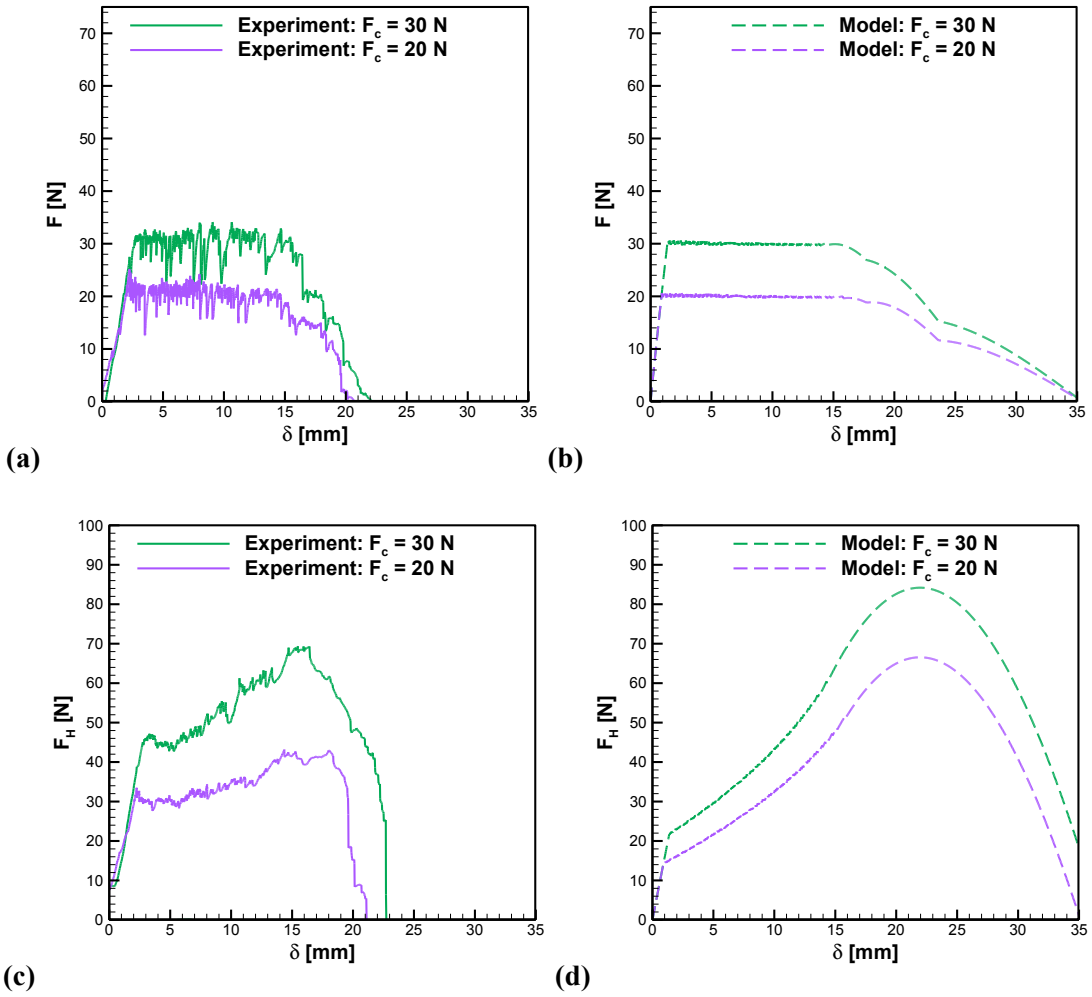

Figure 6: Experimental results and analytical model predictions for K_T^0, $F_c = 20.00$ N and 30.00 N Shown are response for out-of-plane force from (a) experiments, (b) model, and in-plane force from (c) experiments, (d) model in dependence of applied displacement.

Figure 7 compares experimental data and model predictions for K_T^+ and K_T^-, again in terms of out-of-plane and in-plane forces. For the case K_T^+ the agreement of experiment and model is again very good for $\delta < \delta_c$, but a stronger difference between model and experiment is present for $\delta > \delta_c$. For K_T^- predicted out-of-plane forces are in quantitative agreement with model data throughout.

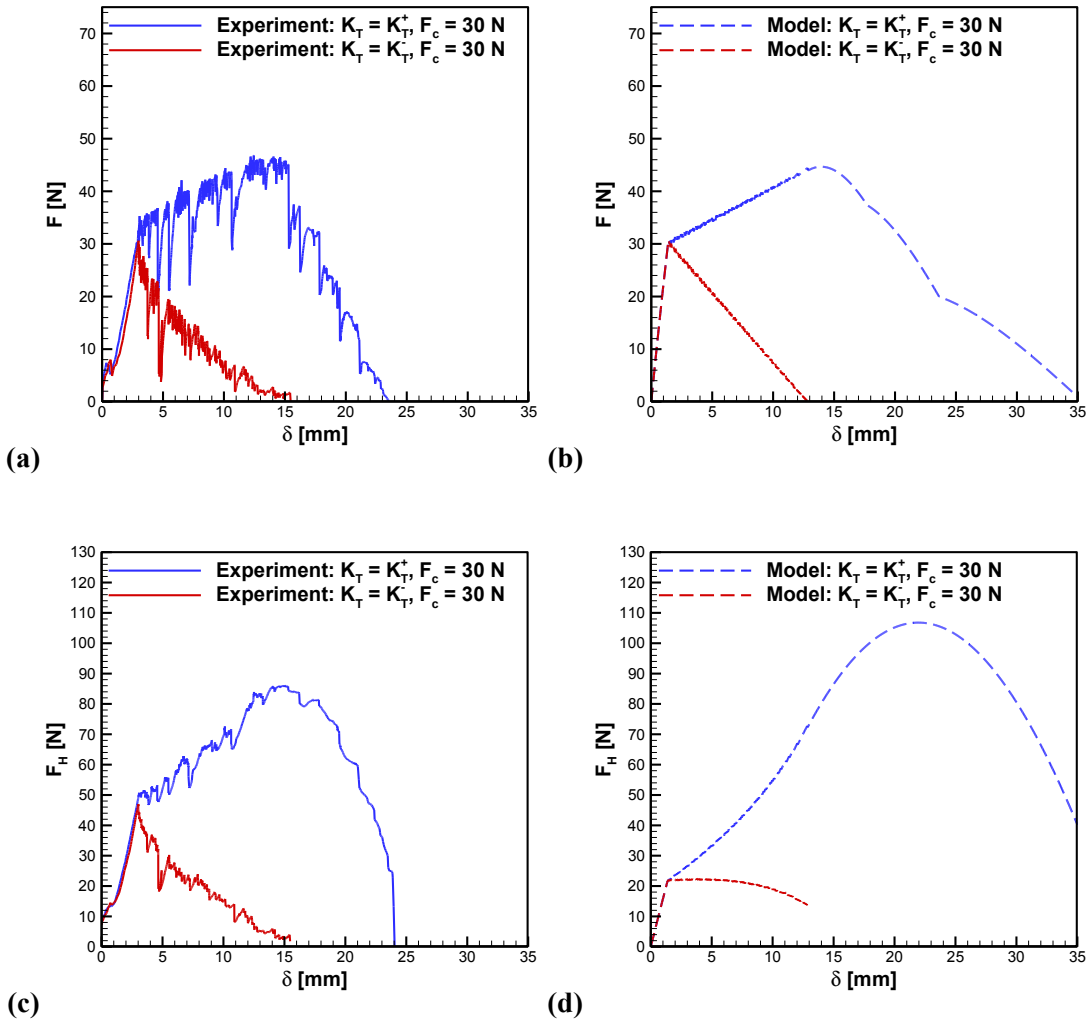

Figure 7: Experimental results and analytical model predictions for K_T^+ and K_T^- with F_c =30.0 N. Response for out-of-plane force from (a) experiments, (b) model, and, in-plane force from (c) experiments, (d) model with increasing applied displacement.

Model predictions of the $F-\delta$ response for various assumed combinations of values of K_T and F_c are depicted in Figure 8. All possible $F-\delta$ responses fall within the envelope given by the $F-\delta$ curve for the case where the initial constraint are maintained throughout. It is also observed that δ_c decreases with

increase in F_c approaching the displacement δ^* at which maximum force F^* is obtained for the case with the fixed constraint.

Figure 9 depicts the overall energy absorption diagram in a format parallel to that developed for cellular solids in [16] for cases K_T^0 and a range of values for F_c. The energy values W are computed as the integrals of $F-\delta$ curves depicted in Figure 8.

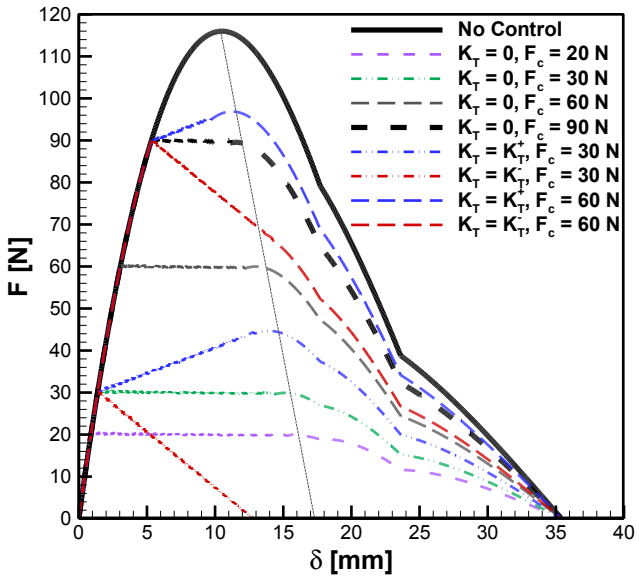

Figure 8: Predicted $F-\delta$ response for different K_T and F_c from the analytical model. The dotted line connects values of δ_c.

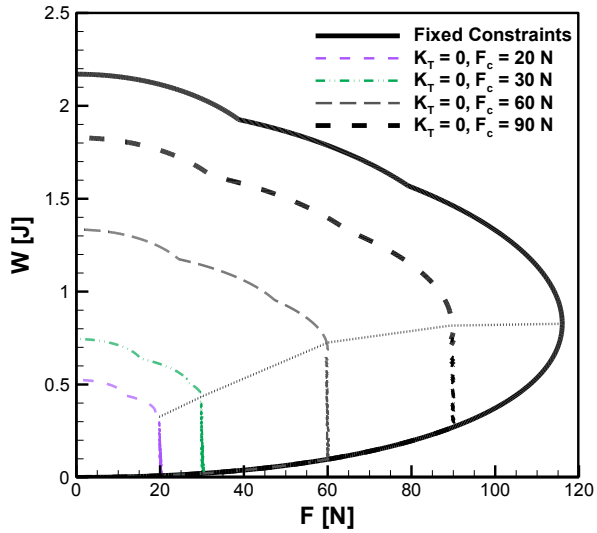

Figure 9: Energy absorption diagram for K_T^0. The dotted line shows maximum W for a given F_c.

The model enables the detailed analysis on the development of the forces in the individual thrust planes. Such analysis allows one to develop an understanding of why and how load transfer in the TIM occurs as the applied displacement increases. Figure 10 shows the out-of-plane components f_V of the thrust forces in planes P_1 to P_3 for K_T^0 and F_c=30.0 N. The overall response of the TIM emerges from the sum of these forces, Eq. 1(b). The three distinct zones emerge from the temporal evolution of the thrust forces in the individual planes. For P_1 the force-deflection response follows the distinct shape of the TIM system under fixed constrains. This is, however, not the case for the forces in thrust planes P_2 and P_3. In these planes the magnitudes of the thrust forces are significantly influenced by the external control of the constraint. In particular forces in P_3 develop non-monotonically.

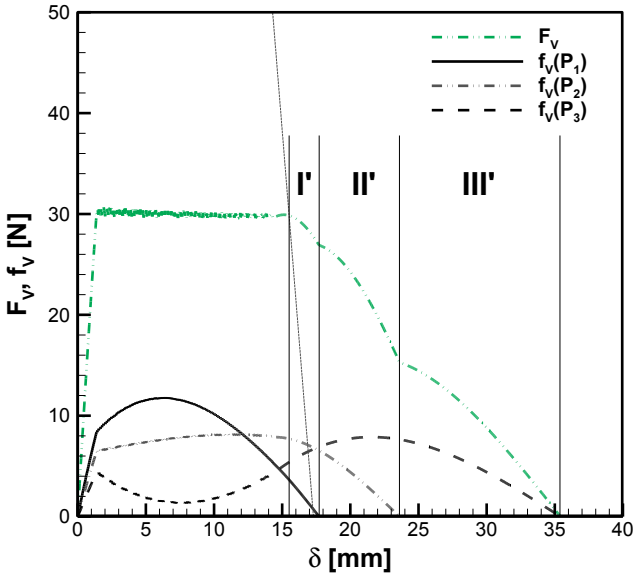

Figure 10: Predicted out-of-plane components f_V of the thrust forces for K_T^0, $F_c = 30.00$ N, together with the overall force-deflection response.

5. DISCUSSION

Optimal energy dissipating structures solve the conflicting requirements of large deformation at low transmitted forces. TIM assemblies provide a means to create such material systems. The present study demonstrates that TIMs can dissipate energy at varying force and stiffness levels, all over large deformations. In contrast, conventional energy dissipating material systems, such as foams, possess each a single response characteristic of plateau stress and densification strain, making it necessary to produce multiple foams materials each acting as an ideal foam for a given load requirement. Using a material like TIM assemblies that can be controlled for the force level under varying load requirements will thus save materials and manufacturing costs. Another main differences that merges between foams and TIMs is the

characteristic of the energy absorption curves, Figure 9. For foams [16], in the late stages of deformation densification leads to a rapid rise in the stress level and thus limits the amount of deformation that can be applied. For TIM assemblies on the other hand, the progressive internal collapse lead to a decline in the transmitted force, still with energy absorption is significantly increasing. Due to this property, TIM assemblies appear as an attractive solution for applications where an increase in transmitted forces cannot be allowed, under any circumstance, to go beyond a critical value while energy dissipation capacity needs to be maintained. In order to make such engineering design selection, however, it is important to gain an understanding of the unique energy dissipation mechanism in TIMs. To this end, a model based on the thrust line analysis approach is presented. The model can be used to compute the TIM response under transverse loading conditions under the consideration of variable constraint. In addition, the conditions of the internal load transfer process can be obtained. Once the model is calibrated, its predictions are found to be in good agreement with the experimental data. Such agreement was seen as particularly good in the early stages of loading but less so in the late stages and during final loss of load carrying capacity. Such differences are contributed to the fact that in experiments friction and slip between unit elements plays a role, but such contributions were neglected in the model. What emerges from the analysis of TIMs is that the internal load transfer is very much alike to the processes during a snap through in a truss system. Yet the key differences between the TIM and a truss system are that in the TIM no tensile stress is present and the internal instability progresses only up to the point where the thrust line are orthogonal to the applied load, and that the topological interlocking between the unit elements prevents the immediate collapse at that instance. The control of the constraint through the adaptive adjustment of boundary conditions enables the control of the load response and the collapse. For the no-slip conditions, as considered in the model,, the mechanical response (stiffness, load carrying capacity, and toughness) of a given TIM (i.e. fixed a_0 and N) under quasi-static loading are uniquely determined by the in-plane constraint force F_{H} and the applied displacement δ. The model thus provides an algorithm based on which a smart material system composed of a TIM assembly, a force and actuator components can function.

6. CONCLUSION

Topologically interlocked material systems are considered as energy dissipating systems with controllable and adaptive mechanical response. A series of experiments were performed to demonstrate the ability of TIM assemblies to provide a desired out-of-plane stiffness lower than the stiffness that might be achieved for the same TIM with fixed abutments. This lower stiffness can be positive, zero or even negative. The maximum force and displacement for adaptive TIM assemblies was found to be limited by the response of the TIM assemblies with fixed constraints. TIM assemblies were shown to possess the ability to

provide constant force over large deformations. Such a material is useful in adaptive energy absorption while keeping low stress levels. The experimental results were replicated using a thrust line based analytical model, similar to the force chain analysis used for 2D granular materials, wherein the in-plane force is controlled by changing the location of boundary and hence truss lengths actively. The model analysis results imply that the force response of the TIMs, for an ideal no-slip condition between unit elements, is directly dependent on the in-plane force and amount of applied transverse displacement. Based on the model a control algorithm for in-plane force actuation in a smart TIM system can be developed. The current model is limited in that slip and frictional energy dissipation can play an additional role in the TIM system response and that such effects will have to be taken into account in further modeling approaches. The present study presents novel strategy to design adaptive energy absorption structures and verifies the concept with experiments and model analysis.

ACKNOWLEDGEMENTS

The authors gratefully acknowledge the support provided for this research by the AFOSR, Program Manager, Dr. Les Lee via Grant# FQ8671-090162. TS acknowledges the support of NSF while working at NSF. The opinions expressed here are solely those of the authors.

REFERENCES

[1] Ashby MF, Brechet YJM 2003 Designing hybrid materials *Acta Materialia* **51** 5801-5821.

[2] Bouaziz O, Brechet YJM, Embury JD 2008 Heterogeneous and architectured materials: A possible strategy for design of structural materials *Advanced Engineering Materials* **10** 24-36.

[3] Fleck NA, Deshpande VS, Ashby MF 2010 Micro-architectured materials: Past, present and future *Proceedings of the Royal Society A* **466** 2495-2516.

[4] Gibson RF 2010 A review of recent research on mechanics of multifunctional composite materials and structures *Composite Structures* **92** 2793-3810.

[5] Ashby MF 2005 Hybrids to fill holes in material property space *Philosophical Magazine* **85** 3235-3257.

[6] Chopra I 2002 Review of state of art of smart structures and integrated systems *American Institute of Aeronautics and Astronautics Journal* **40** 2145-2187.

[7] Garg DP, Zikry MA, Anderson LA 2001 Current and potential future research activities in adaptive structures: An ARO perspective *Smart Materials and Structures* **10** 610-623.

[8] Mcknight G, Doty R, Keefe A, Herrera G, Henry C 2010 Segmented reinforcement variable stiffness materials for reconfigurable surfaces *Journal of Intelligent Material Systems and Structures* **21** 1783-1793.

[9] Spillman Jr WB, Sirkis JS, Gardiner PT 1996 Smart materials and structures: What are they? *Smart Materials and Structures* **5** 247-254.

[10] Thompson BS, Gandhi MV, Kasiviswanathan S 1992 An introduction to smart materials and structures *Materials and Design* **13** 3-9.

[11] Ashby MF, Brechet YJM, Cebon D, Salvo L 2003 Selection strategies for materials and processes *Materials and Design* **25** 51-67.

[12] Brechet YJM, Bassetti D, Landru D, Salvo L 2001 Challenges in materials and process selection *Progress in Materials Science* **49** 407-428.

[13] Lu G, Yu TX 2003 Energy absorption of materials and structures *Woodhead Publishing Limited, Cambridge, UK.*

[14] Alghamdi AAA 2001 Collapsible impact energy absorbers: An overview *Thin-Walled Structures* **39** 189–213.

[15] Gao ZY 2005 Dynamic behavior of cellular materials and cellular structures: Experiments and modeling *PhD Thesis, The Hong Kong University of Science and Technology, Hong Kong*.

[16] Gibson LJ, Ashby MF 1997 Cellular Solids: Structure and properties *Second Ed. Cambridge University Press, Cambridge, UK*.

[17] Karagiozova D, Yu TX, Gao ZY 2007 Stress-strain relationship for metal hollow sphere materials as a function of their relative density *Journal of Applied Mechanics* **74** 898-907.

[18] Carruthers JJ, Kettle AP, Robinson AM 1998 Energy absorption capability and crashworthiness of composite material structures: A review *Applied Mechanics Reviews* **51** 635-649.

[19] Farley G L 1983 Energy absorption of composite materials *Journal of Composite Materials* **17** 267-279.

[20] Thornton PH 1979 Energy absorption in composite structures *Journal of Composite Materials* July **13** 247-262.

[21] Holnicki-Szulc J, Knap L 2004 Adaptive crashworthiness concept *International Journal of Impact Engineering* **30** 639-663.

[22] Mahmood SAJHF, Baccouche MR 1999 Smart structure for improving crashworthiness in vehicle frontal collisions *ASME International Mechanical Engineering Congress Expo, Nashville, Tennessee, United States* 135-144.

[23] Angioni SL, Meo M, Foreman A 2011 Impact damage resistance and damage suppression properties of shape memory alloys in hybrid composites: A review *Smart Materials and Structures* **20** 013001.

[24] Holnicki-Szulc J, Pawlowski P, Wiklo M 2003 High-performance impact absorbing materials—the concept, design tools and applications *Smart Materials and Structures* **12** 461-467.

[25] Dyke SJ, Spencer Jr BF, Sain MK, Carlson JD 1996 Modeling and control of magnetorheological dampers for seismic response reduction *Smart Materials and Structures* **5** 565-575.

[26] Yang G, Spencer Jr BF, Carlson JD, Sain MK 2002 Large-scale MR fluid dampers: Modeling and dynamic performance considerations *Engineering Structures* **24** 309-323.

[27] Deshmukh SS, McKinley GH 2007 Adaptive energy-absorbing materials using field-responsive fluid-impregnated cellular solids *Smart Materials and Structures* **16** 106-113.

[28] Wereley NM, Choi YT, Singh HJ 2011 Adaptive Energy Absorbers for Drop-induced Shock Mitigation *Journal of Intelligent Material Systems and Structures* **22** 515-519.

[29] Dyskin AV, Estrin Y, Kanel-Belov AJ, Pasternak E 2003a A new principle in design of composite materials: Reinforcement by interlocked elements *Composites Science and Technology* **63** 483-491.

[30] Khor HC 2008 Mechanical and structural properties of interlocking assemblies *PhD Thesis, The University of Western Australia, Perth, Australia.*

[31] Molotnikov A, Estrin Y, Dyskin AV, Pasternak E, Kanel-Belov AJ 2007 Percolation mechanism of failure of a planar assembly of interlocked osteomorphic elements *Engineering Fracture Mechanics* **74** 1222-1232.

[32] Estrin Y, Dyskin AV, Pasternak E 2011 Topological interlocking as a material design concept *Materials Science Engineering: C* **31** 1189-1194.

[33] Schaare S, Dyskin AV, Estrin Y, Arndt S, Pasternak E, Kanel-Belov A 2008 Point loading of assemblies of interlocked cube-shaped elements *International Journal of Engineering Science* **46** 1228-1238.

[34] Dyskin AV, Estrin Y, Kanel-Belov AJ, Pasternak E 2001 A new concept in design of materials and structures: Assemblies of interlocked tetrahedron-shaped elements *Scripta Materialia* **44** 2689-2694.

[35] Dyskin AV, Estrin Y, Kanel-Belov AJ, Pasternak E 2003b Topological interlocking of platonic solids: A way to new materials and structures *Philosophical Magazine Letters* **83** 197-203.

[36] Dyskin AV, Estrin Y, Pasternak E, Khor HC, Kanel-Belov AJ 2003c Fracture resistant structures based on topological interlocking with non-planar contacts *Advanced Engineering Materials* **5** 116-119.

[37] Mather A, Cipra RJ, Siegmund T 2011 Structural integrity during remanufacture of a topologically interlocked material *International Journal of Structural Integrity* **3** 61-78.

[38] Khandelwal S, Siegmund T, Cipra RJ, Bolton JS 2012 Transverse loading of cellular topologically interlocked materials *International Journal of Solids and Structures* **49** 2394-2403.

[39] Liao CL, Chan TC, Suiken ASJ, Chang CS 2000 Pressure-dependent elastic moduli of granular assemblies International Journal for Numerical and Analytical Methods in Geomechanics **24** 265-279. .

[40] Brown E, Rodenberg N, Amend J, Mozeika A, Steltz E, Zakin MR, Lipson H, Jaeger HM 2010 Universal robotic gripper based on the jamming of granular material *Proceedings of the National Academy of Sciences* **107** 18809-18814.

[41] Follmer S, Leithinger D, Olwal A, Cheng N, Ishii H 2012 Jamming user interfaces: Programmable particle stiffness and sensing for malleable and shape-changing devices *Proceedings of the 25th Annual ACM Symposium on User Interface Software and Technology* 519-528.

[42] Goldenberg C, Goldhirsch I 2002 Force chains, microelasticity, and macroelasticity *Physical Review Letters* **89** 084302.

[43] Mueggenburg KE, Jaeger HM, Nagel SR 2002 Stress transmission through three-dimensional ordered granular arrays *Physical Review E* **66** 031304.

[44] Khandelwal S, Siegmund T, Cipra RJ, Bolton JS 2013 Scaling of the Elastic Behavior of 2D Topologically Interlocked Materials under Transverse Loading *Journal of Applied Mechanics* **81** 031011.

[45] Conway JH, Torquato S 2006 Packing, tiling and covering with tetrahedra *Proceedings of the National Academy of Sciences* **103** 10612-10617.

[46] Humphreys JS 1966 On dynamic snap buckling of shallow arches *American Institute of Aeronautics and Astronautics Journal* **4** 878-886.

[47] Hsu CS 1968 Equilibrium configurations of a shallow arch of arbitrary shape and their dynamic stability character *International Journal of Non-linear Mechanics* **3** 113-136.